

Article

Degradation and Breakdown of Polymer/Graphene Composites under Strong Electric Field

Yangming Kou, Xiang Cheng  and Christopher W. Macosko *

Department of Chemical Engineering and Materials Science, University of Minnesota, 421 Washington Avenue SE, Minneapolis, MN 55455, USA; kouxx036@umn.edu

* Correspondence: xcheng@umn.edu (X.C.); macosko@umn.edu (C.W.M.)

Abstract: In this work, we study the effect of strong electric fields on a polymer/graphene composite and the resulting morphology upon its dielectric breakdown. Our model system was produced by compounding up to 0.25 wt% graphene nanoplatelets (GNP) into poly(ethylene-co-vinyl acetate) (EVA), which is a soft polymer with low melt viscosity. A strong electric field of up to 400 V_{rms}/mm was applied to the EVA/GNP composite in the melt. The sample's resistance over the electric field application was simultaneously measured. Despite the low GNP loading, which was below the theoretical percolation threshold, the electric conductivity of the composite during electric field application dramatically increased to >10⁻⁶ S/cm over 5 min of electric field application before reaching the current limit of the experimental apparatus. Conductivity growth follows the same scaling relationship of the theoretical model that predicts the rotation and translation time of GNPs in a polymer melt as a function of electric field strength. Since no significant GNP alignment in the composite was observed under transmission electron microscopy (TEM), we hypothesized that the increase in electrical conductivity was due to local electrical treeing of the polymer matrix, which eventually leads to dielectric breakdown of the composite. Electrical treeing is likely initiated by local GNP agglomerates and propagated through conductive channels formed during progressive dielectric breakdown.

Keywords: graphene; electric field; polymer composite; degradation



Citation: Kou, Y.; Cheng, X.; Macosko, C.W. Degradation and Breakdown of Polymer/Graphene Composites under Strong Electric Field. *J. Compos. Sci.* **2022**, *6*, 139. <https://doi.org/10.3390/jcs6050139>

Academic Editor: Francesco Tornabene

Received: 11 April 2022

Accepted: 5 May 2022

Published: 10 May 2022

Publisher's Note: MDPI stays neutral with regard to jurisdictional claims in published maps and institutional affiliations.



Copyright: © 2022 by the authors. Licensee MDPI, Basel, Switzerland. This article is an open access article distributed under the terms and conditions of the Creative Commons Attribution (CC BY) license (<https://creativecommons.org/licenses/by/4.0/>).

1. Introduction

Most polymers are good electrical insulators. Since macromolecular chains are held together by covalent bonds, electron transport through most polymers is poor. Adding hard filler particles to a host polymer matrix can further improve their material properties such as increased toughness and hardness, and resistance to heat and chemicals. As such, polymer composites containing inorganic insulating fillers such as glass, silica, and alumina are widely used in industry for electrical insulation applications, from low-voltage home appliances to high-voltage power grids [1,2]. In order to design polymer composites that are safe and provide adequate dielectric strength for high-voltage applications, the phenomenon of electric field-induced breakdown of particle-reinforced polymers is well-studied [3,4]. Conductive polymer composites, on the other hand, are a different class of materials, produced by loading electrically conductive particles into a host polymer. Conductive polymer composites are applied in electrostatic discharge protection and electromagnetic interference shielding. In their application, these composites may be temporarily exposed to high instantaneous electric fields created by static electricity or the surrounding environment [5]. The resultant electrical current may lead to potential electrical breakdown and material failure, thereby posing significant safety risks. However, the effect of electric field on the possible breakdown of conductive polymer composites containing electrically conductive fillers is not well understood. Therefore, studying the effect of the electric field on conductive polymer composites could offer insights into the

electrical breakdown mechanism for this class of materials, thereby better informing their design and application in high-voltage environments.

Applying an electric field is also a powerful method to modify the microstructure of soft materials and control material properties for practical applications. In a number of previous studies related to the construction of conductive polymer composites, alternating electric fields were utilized to align conductive fillers such as carbon black [6], graphite flakes [7–9], carbon nanotubes [10], and graphene nanoplatelets (GNPs) [11] in liquids such as uncured polyester resin or epoxy. Under the electrical field, filler particles can undergo alignment with the electric field to create composites with anisotropic material properties including higher tensile modulus, electrical conductivity, thermal conductivity, and fracture toughness in the field direction. Electric fields of low to medium strength (10^1 – 10^2 V/mm) were used to control the dispersion and orientation of conductive fillers in low viscosity media (~ 1 Pa·s at room temperature) [6,11–13]. There was no attempt to use strong electric fields to directly modify the morphology of molten polymer composites with much higher viscosities (e.g., $\sim 10^2$ – 10^4 Pa·s at 150–250 °C).

In this work, we study the effects of a strong electric field (up to 400 V_{rms} /mm) when applied to a conductive polymer/GNP composite in the melt state. We measure the time-resolved electrical conductivity of the composite by systematically varying the applied field strength and GNP concentration. We performed complementary transmission electron microscopy and dielectric rheology experiments before and after electric field application. These methods allow us to characterize the morphology and filler orientation of the composites, and determine whether electrical breakdown occurs. In addition, we quantitatively compare our experimental results to a model describing individual GNP rotation and translation under an alternating electric field. Our results suggest that GNP alignment may occur in local GNP agglomerates where local electrical conductivity is high and dielectric strength is low. These regions could promote electrical treeing formation in the surrounding polymer dielectric. Electrical treeing causes polymers to degrade and leads to channel formation, ultimately resulting in the dielectric breakdown of the bulk composite.

2. Experimental Section

2.1. Polymer Blend Preparation

Poly(ethylene-co-vinyl acetate) (EVA, Elvax 40 W, 40 wt% vinyl acetate, density = 0.965 g/cm³) was obtained from the Dow Chemical Company. EVA was dried in a vacuum oven at 40 °C for at least 12 h prior to use. Graphene nanoplatelets (GNPs, N002-PDR) were obtained from Angstrom Materials (Dayton, OH, USA), and their material characteristics are reported in our previous publication [14–17]. Probe sonication was used to disperse and exfoliate GNPs in tetrahydrofuran (THF, reagent grade, Sigma-Aldrich, St. Louis, MO, USA). In a centrifuge tube, the desired amount of GNP was added into ~ 40 mL of THF. Then, the resulting suspension was continuously probe-sonicated (Branson Digital Sonifier SFX 250, Danbury, CT, USA) using a $\frac{1}{4}$ inch probe at 75 W for 1 h under an ice water bath. In a separate container, 4 g of EVA was dissolved in 40 mL of THF. Then, the sonicated GNP suspension was added into the EVA/THF solution and stirred at room temperature for 5 min, followed by coprecipitation into ~ 500 mL of methanol (reagent grade, Sigma-Aldrich). The resulting composite was filtered and dried in vacuo for at least 24 h to remove THF. This was pressed into 1 mm thick sheets by compression molding using a hot press (Wabash Carver Press, Wabash, IN, USA) at 180 °C and ~ 9 MPa pressure. Lastly, sample swatches were cut using a 3 mm diameter circular die punch.

2.2. Electric Field Application with Heating Stage

The electric field was applied to the polymer melt using a PC-controlled high-voltage sequencer (LabSmith, HVS448-1500, Livermore, CA, USA) in conjunction with a heating stage (Figure 1a). LabSmith Sequence PC software was used to generate a sinusoidal voltage while simultaneously recording voltage and current. The rate of data sampling

and recording was 16 Hz. The composite sample was inserted into a circular hole of 3 mm diameter at the center of a 1 mm insulating silicone rubber spacer, which was then sandwiched between two copper electrodes. An image of the sample is given in Figure 1b. Copper wires were soldered onto the electrodes, which were in turn connected to the sequencer. The entire sandwich was placed on top of a homemade stainless-steel heating stage, constructed using a flexible heating element (40 W, 10 W/in², Omega Engineering, Norwalk, CT, USA) and a PID temperature controller (Omega Engineering). An electric field was applied after the composite sample had been heated to 160 °C to reduce the viscosity of the polymer matrix. The electric field was applied until the maximal allowable current (~3–10 mA) had been reached, when part of the sample was burnt through. Smoke emitted from the sample, and the remaining sample always contained a hole (Figure 1c).

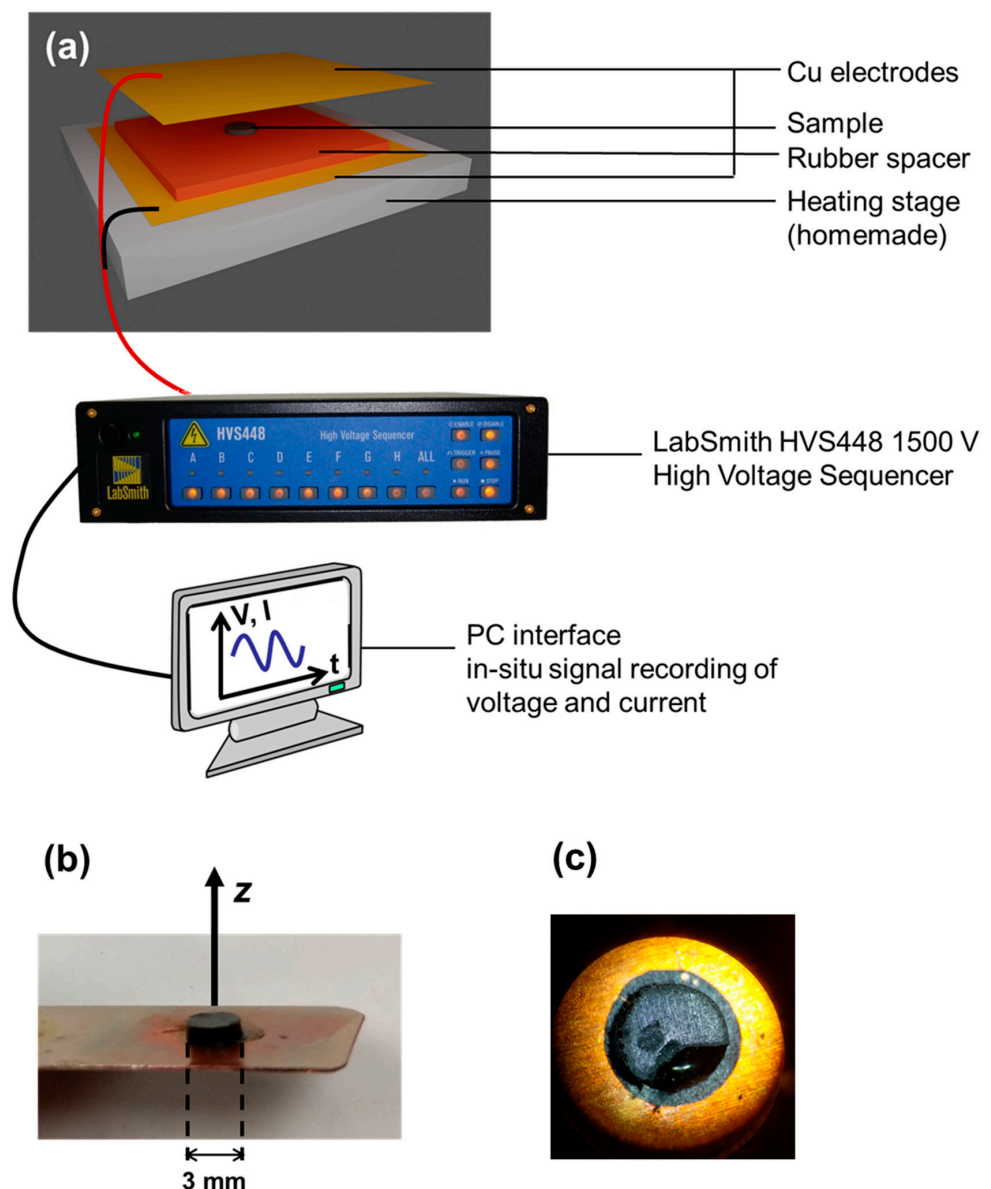


Figure 1. (a) Experimental setup for electric field application to polymer melt. (b) Test specimen of EVA/GNP_0.25 wt% mounted on a Cu electrode prior to electric field application. Sample dimension and electric field direction (z) denoted. (c) Test specimen after electric field application. Polymer degradation occurred in part of the sample (lower right portion of the image showing a hole).

2.3. Characterization with Transmission Electron Microscopy

After electric field application, the sample was rapidly quenched to below the glass transition temperature using dry ice. Then, the sample was carefully removed from the sandwich and embedded in epoxy resin, which was cured at room temperature. Ultrathin (~90 nm) sections were obtained by cryomicrotomy (Leica UC6, Wetzlar, Germany) at $-140\text{ }^{\circ}\text{C}$ using a diamond knife. Sample sections were prepared in the plane parallel to the direction of electric field application. Bright-field transmission electron microscopy (TEM) images were obtained using a FEI Tecnai G2 Spirit BioTWIN microscope (Hillsboro, OR, USA) with an accelerating voltage of 120 kV. In the TEM images, the horizontal stripe features represent knife marks (artifacts from cryomicrotomy) and are parallel with the direction of the applied electric field.

3. Results

3.1. Direct Electrical Conductivity Measurement during Electric Field Application

The electrical conductivity of the EVA/GNP composite was measured continuously during electric field application. Figure 2a shows the time-resolved raw voltage and current signals as measured by the high-voltage sequencer across three EVA/GNP_0.25 wt% samples in the field direction. Electric field strength was $E_0 = 400\text{ V}_{\text{rms}}/\text{mm}$ and $\omega_{\text{AC}} = 1\text{ s}^{-1}$. Since the voltage and current signals were in phase with each other, the composite effectively acted as a resistor in the AC circuit. The conductivity of the composite (σ_z , in S/cm measured in the axial (z) direction based on the setup given by Figure 1) was calculated using Ohm's law:

$$\sigma_z = \frac{d \cdot I}{A \cdot V}, \quad (1)$$

where d is the thickness (0.1 cm) and A the surface area (0.08 cm²) of the composite, and I and V are the current and voltage signals from the high-voltage sequencer, respectively. The time-resolved electrical conductivities of the three samples are shown in Figure 2b. Current resolution was $\pm 10\text{ }\mu\text{A}$, representing the background noise of the sequencer. On the basis of the sample geometry, this corresponds to a lower current detection limit of $\sim 2 \times 10^{-8}\text{ S/cm}$. Results from Figure 2b suggest that the electrical conductivity of EVA/GNP composite increased exponentially as a function of time when the electric field was turned on. Then, the increase in electrical conductivity became slower once the conductivity had reached $\sim 10^{-6}\text{ S/cm}$. The sequencer reached its current limit ($\sim 5\text{ mA}$) at 3–5 min of electric field application. When the electrical current through the sample was above 1 mA, the current signal became unstable, fluctuated widely, and triggered the internal circuit mechanism of the sequencer to shut off the applied electric field. Therefore, the maximal electrical conductivity the composite was reached using the high-voltage sequencer occurs between 10^{-6} and 10^{-5} S/cm . In comparison, the neat EVA polymer exhibited insulating behavior when an alternating electric field was applied in the molten state for over 20 min (Figure 3). Voltage and current signals were out of phase with each other, and the AC current fell completely within the range of instrument background noise ($< 10\text{ }\mu\text{A}$). Given that there were no current conducting species, this behavior was as expected for a neat polymer matrix. The difference in the time-dependent electrical conductivity between EVA/GNP composite and EVA neat polymer during electric field application suggested that the electric field imparted microstructural changes to the conductive GNPs within the composite.

Lastly, we measured time-resolved conductivity change to the EVA/GNP composite by changing the electrical field strength (Figure 4a), temperature (Figure 4b), or GNP concentration (Figure 4c). Results show that EVA/GNP composites required a longer time until electrical breakdown when electric field strength, temperature, or GNP concentration was lowered. For all samples shown in Figure 4 (except for the EVA/GNP_0.05 wt% shown in Figure 4c), conductivity measurement was stopped due to electrical breakdown when smoke was emitted from the sample, and a hole through the sample was created (Figure 1c). Lastly, the onset of electrical current increase showed sample-to-sample variations, likely

from the inherent inhomogeneity in graphene dispersion between swatches. Nonetheless, the rate of current increase was comparable once the current reading was above the instrument’s detection limit.

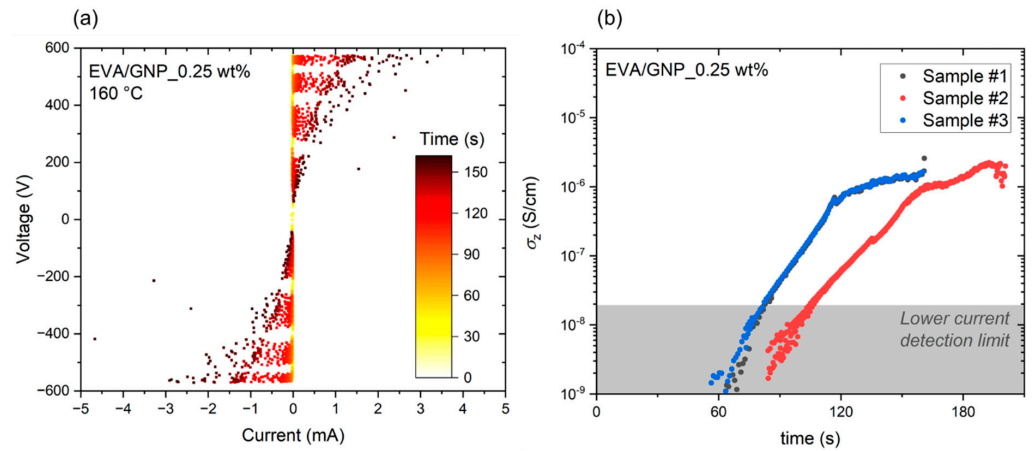


Figure 2. Time-resolved (a) voltage and current signals for Sample 1; (b) through-direction electrical conductivities of three EVA/GNP_0.25 wt% samples during application of alternating electric field of $E_0 = 400 \text{ V}_{\text{rms}}/\text{mm}$ and $\omega_{\text{AC}} = 1 \text{ s}^{-1}$. For all three samples, time zero was determined with the time at which the electric field was switched on.

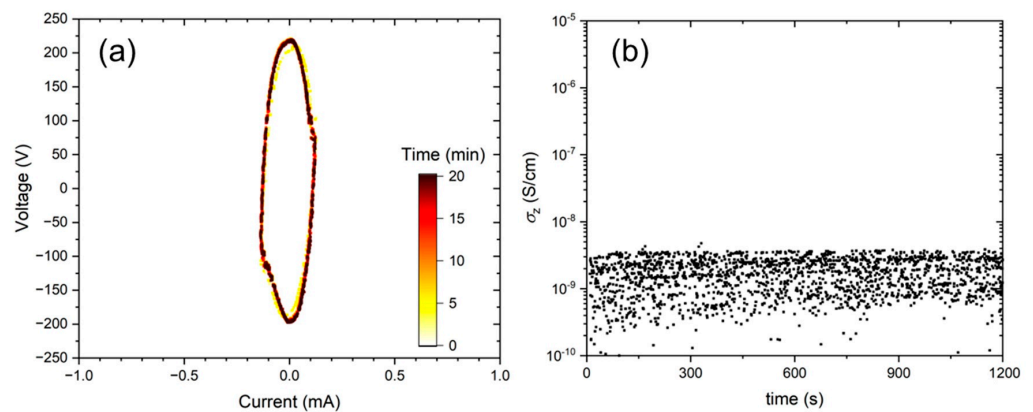


Figure 3. (a) Current–voltage characteristic behavior of EVA neat polymer at 160 °C under an alternating electric field of $E_0 = 150 \text{ V}_{\text{rms}}/\text{mm}$ and $\omega_{\text{AC}} = 1 \text{ s}^{-1}$. Cyclic hysteresis curve suggested that the EVA melt was an insulator and did not undergo dielectric breakdown. (b) Through-direction electrical conductivity at sequencer noise level.

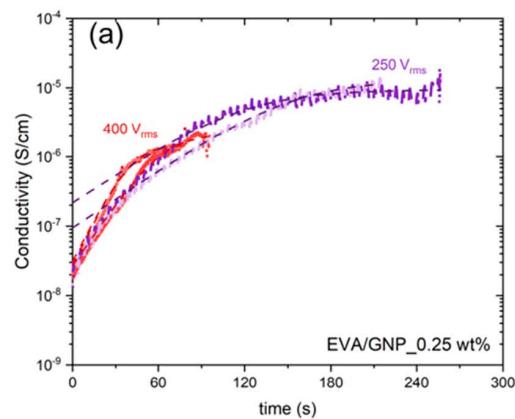


Figure 4. Cont.

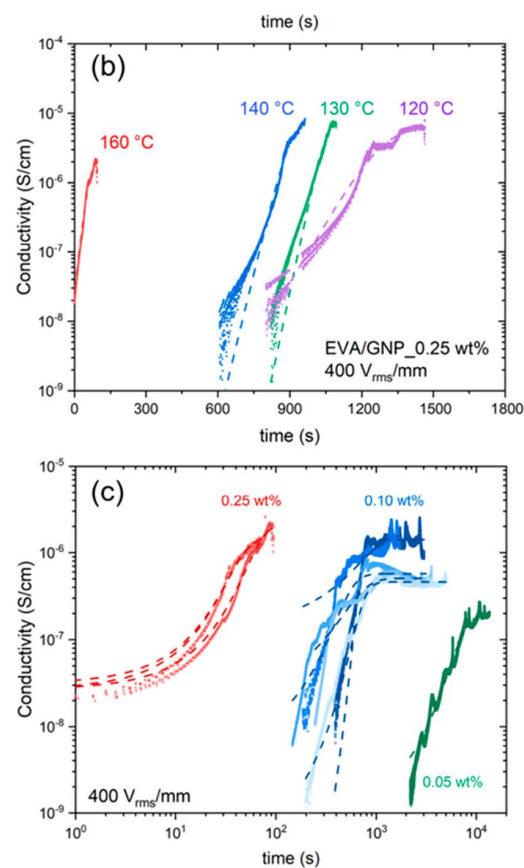


Figure 4. Time-resolved electrical conductivity of EVA/GNP composites during electric field application. (a) GNP concentration fixed at 0.25 wt% with varying electric field strength (400 V_{rms}/mm or 250 V_{rms}/mm) at 160 °C. (b) Field strength fixed at 400 V_{rms}/mm with varying temperature (120–160 °C) to control composite melt viscosity. (c) Field strength fixed at 400 V_{rms}/mm with varying GNP concentrations (0.25, 0.10, or 0.05 wt%); dashed line, fitting with the logistic growth model given by Equation (5).

3.2. TEM Imaging of Composites after Electric Field Application

Next, TEM imaging of the EVA/GNP composites was performed to evaluate whether electric field application changed the microstructural morphology of the composite. Due to the softness of the EVA polymer and the black visual appearance of the EVA/GNP composite, characterization with the naked eye or optical microscopy was not possible. On the other hand, TEM allows for the direct visualization of GNP dispersion and orientation within the blend. Cryomicrotomy was performed in the plane of the electric field application after a portion of bulk sample had been embedded in an epoxy matrix. During cryomicrotomy, small defects on the diamond knife cutting edge create two types of artifacts that help in identifying the direction of the electric field application (Figure A1). The first type of artifact is knife marks, shown as the sparse patterns which orient perpendicular to the knife's cutting edge. The second type of artifacts is chattering that arises from sample vibration and irregular compression between specimen cutting face and knife edge. This produces dense patterns that orient parallel to the knife's cutting edge. Figure 5 shows representative TEM images of EVA/GNP_0.25 wt% samples before and after electric field application. No percolating GNP network was observed in either sample because the GNP concentration was below the percolation threshold for a homopolymer matrix (~0.5 wt% based on our previous work [17]).

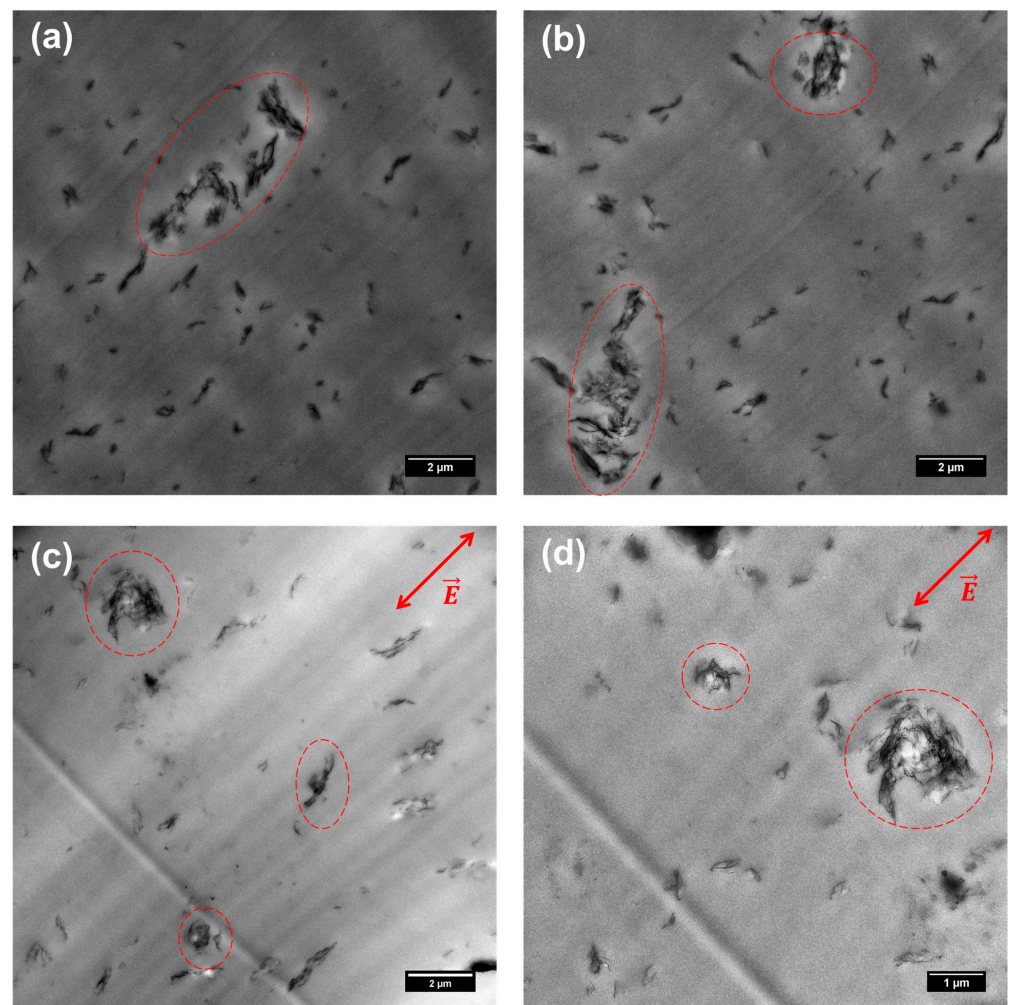


Figure 5. TEM images of EVA/GNP_0.25 wt% samples (a,b) before and (c,d) after 100 s electric field application ($E_0 = 400 \text{ V}_{\text{rms}}/\text{mm}$ and $\omega_{\text{AC}} = 1 \text{ s}^{-1}$). (c,d) Direction of the alternating electric field determined by microtome artifacts. Locations of locally aggregated GNPs are highlighted by dashed circles.

4. Discussion

Next, we discuss two possible hypotheses related to the electrical conductivity increase in EVA/GNP composites under the applied electric field. First, we discuss whether GNPs could become aligned under the electric field, which leads to the increase in bulk electrical conductivity increase. Next, we discuss the effect of localized electrical treeing formation during dielectric breakdown could induce an increase in electrical conductivity.

4.1. GNP Alignment-Induced Conductivity Increase

Small particles such as GNPs can be aligned under an electric field via dielectrophoresis. In order to evaluate whether an individual GNP aligned under our experimental conditions, we applied the model proposed by Wu et al. [11]. We modeled EVA/GNP composite as a dielectric matrix with conductive solid inclusions. The application of a sinusoidal alternating electric field can result in both rotational and translational movement to an individual GNP nanosheet. Assume that an individual GNP sheet is initially oriented at angle θ_0 relative to the electric field and placed at distance x_0 from another GNP sheet.

In response to the field, this GNP sheet first requires a rotation time (t_r) to be fully aligned within 1° with the field direction:

$$t_r = \frac{8\eta\left(\frac{\pi}{2} - \frac{b}{a}\right)}{\pi\epsilon_m E_0^2} \ln \frac{\tan \theta_0}{\tan 1^\circ}. \tag{2}$$

Once it becomes aligned with the field, it requires additional translation time (t_c) to form an end-to-end connection with the adjacent GNP sheet, which can be estimated as follows:

$$t_c = \frac{\eta k_t \epsilon_0}{\pi a^4} \left(\frac{\pi}{2} - \frac{b}{a}\right)^2 \frac{x_0^3}{E_0^2 \epsilon_m^2}. \tag{3}$$

The detailed derivations of these equations can be found in [11]. The following values relevant to our EVA/GNP system were used in our calculations: a and b refer to the lateral dimension ($\sim 1 \mu\text{m}$) and thickness ($\sim 1 \text{ nm}$) of individual GNP sheets, respectively. The melt viscosity of the EVA matrix at 160°C was $\eta = 450 \text{ Pa}\cdot\text{s}$ (experimentally measured with ARES-2 rheometer); $E_0 = 400 \text{ V}_{\text{rms}}/\text{mm}$ is the strength of the electric field; $\epsilon_m = 6.7 \epsilon_0$ is the dielectric constant of the EVA matrix (experimentally measured using the dielectric rheology accessory at processing temperature); k_t is the translational friction coefficient of GNP given as follows [18]:

$$k_t = 6\pi(a^2b)^{\frac{1}{3}} \frac{\left|(b/a)^2 - 1\right|^{\frac{1}{2}}}{\tan^{-1}\left(\frac{\left|(b/a)^2 - 1\right|^{\frac{1}{2}}}{(b/a)}\right)}. \tag{4}$$

Our calculation shows that commanding 5 min of $400 \text{ V}_{\text{rms}}/\text{mm}$ was sufficient to align GNP sheets within 15° of the electric field direction (Figure 6). Once GNPs became aligned, end-to-end connection of two adjacent sheets that were separated by a few micrometers was formed within seconds, which leads to the formation of a conducting network in the field direction (Figure 6).

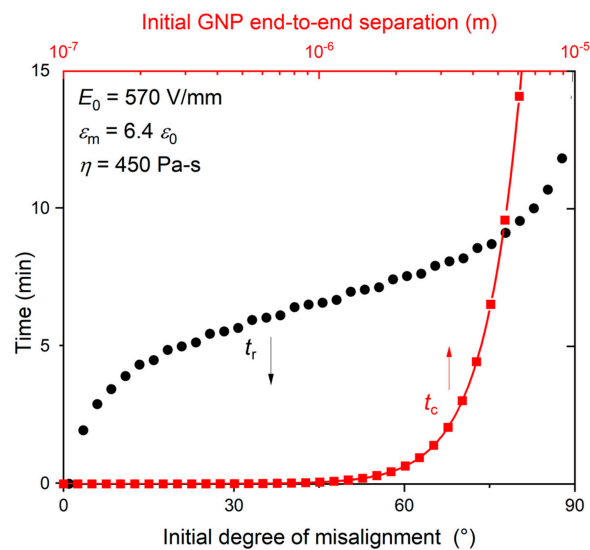


Figure 6. Rotational time (in black, t_r) required for individual GNP to become aligned with electric field as a function of initial degree of misalignment (bottom x-axis), and translational connection time (in red, t_c) for two aligned GNP to form end-to-end connection as a function of initial distance of separation (top x-axis). The melt viscosity and dielectric constant of the polymer matrix correspond to our EVA/GNP composite at 160°C under the experimental conditions.

However, TEM results in Figure 5 show that applying the electric field to the EVA/GNP melt did not result in global GNPs alignment. Contrary to the model that assumes a single GNP sheet in the polymer matrix, GNPs in the composite were local agglomerates (highlighted as dashed circles). Even though blends were prepared by extensive probe sonication and solution blending, GNPs were not fully exfoliated due to the strong π - π interactions between sheets. Therefore, the Wu model that describes individual graphene alignment under the electric field does not adequately describe the present system. The strong interparticle interaction causes GNP agglomeration, which reduces the polymer/particle interfacial volume and reduces the particles' ability to improve the composites' dielectric properties. Modifying nanoparticle-polymer interaction can lead to changes in the final composites' material properties, such as rheology, mechanical properties, particle dispersibility, and dielectric strength [19–22]. Increased particle-polymer interaction changes both the polymer morphology and local charge distribution at the polymer-nanoparticle interface, thereby improving the composites' dielectric properties. Siddabattuni et al. demonstrated that the dielectric constants of TiO₂/epoxy composites can be controlled by modifying TiO₂ surfaces with self-assembled monolayer organophosphate ligands with different chemical functionalities [22]. However, the chemical functionalization of neat graphene sheets is difficult due to the strong sp² hybridization of carbon structure and can lead to the decreased electrical conductivity of graphene nanoparticles.

We performed statistical analysis on the TEM images of EVA/GNP blends after electric field application (Figure 5c,d) on the orientation of the GNP sheets, but found no correlation between GNP orientation and electric field direction. After electric field application, we extracted the orientation angle of each individual GNP sheet (total number of sheets was ~150) within a single TEM image. The standard deviation of the orientation angle was $\pm 52^\circ$ relative to the mean angle of orientation, suggesting that the sheets were still randomly oriented over a wide distribution. Additionally, the mean angle of GNP orientation was $\sim 40^\circ$ different from the electric field direction. This evidence suggests that the electric field had a much weaker effect on inducing the alignment of GNP aggregates than that of individual GNP sheets. Therefore, the effect of electric field on the composite was localized. Since TEM imaging only provides a limited field of view (on the order of $\sim 10 \mu\text{m}^2$) whereas the cross-sectional area of the test specimen is $\sim 8 \text{mm}^2$, it is possible that the actual conductive pathway induced by electric field application occurred in a different area. Nevertheless, should the electric field induce global effects on the composite such as graphene orientation, these effects would be observed throughout the composite regardless of the specific area being examined.

4.2. Dielectric Breakdown Induced Conductivity Increase

Another hypothesis that explains the observed increase in electrical conductivity during electric field application is due to the samples' dielectric breakdown. When the sample was removed from the electrodes after reaching the maximal allowed current from the sequencer, a cavity was found towards the edge of nearly all our samples (Figure 1c). Additionally, upon reaching the maximum allowable current, smoke would emit from the sample. The smoke indicated that the polymeric composite underwent electrical and thermal degradation, which ultimately caused soot particles to be formed [23]. These observations suggest dielectric breakdown of the sample occurred due to the electric field.

The dielectric breakdown of polymers by tree propagation due to an external electric field can be described in three stages [24]. First, tree inception occurs from a point of a high local electric field near the electrode. This process is usually enhanced by the presence of local defects in the composite, such as cavities in the dielectric medium, the presence of conductive fillers near the surface, roughness of the contacting electrode, and partial discharge activities [3,25]. Second, tree growth is initiated by the partial discharge of polymer surface that leads to surface erosion and decrease in material thickness. The loss of material could come from a number of processes related to electric field applications, such as direct ion bombardment, localized heating due to gases generated by the degradation

of polymers to CO₂, and excitation and oxidation of surface molecules [4]. Eventually, electric-field-induced surface erosion creates small channels that penetrate the polymer matrix, forming the first conductive bridge across the two electrodes [25]. Third, as a conductive pathway is formed between the two electrodes, small and branched channels are widened. Electrical conductivity continues to increase until dielectric breakdown. The early stages of electrical treeing and channel growth are often modeled as a stochastic process that is proportional to the electric field strength [20,26].

Nonetheless, electrical treeing at high field strengths can be deterred by adding well-dispersed insulating inorganic particles (e.g., silica, titanium dioxide, aluminum oxide, silicon carbide) into the polymer matrix. This enhances the dielectric strength of the host polymer, creating functional materials for high-voltage insulation ($>10^3$ V/mm) applications. When insulating nanoparticles are well-dispersed in a polymer matrix, the large interfacial area between the particle and the host matrix and the small interparticle distance both provide physical barriers that impede the flow of electric current between two electrodes (Figure 7a). For conductive fillers, Han et al. found that their dispersion state strongly affects the rate of electrical treeing in polymer nanocomposites [27]. In graphene/silicone rubber systems, a small amount (~ 0.005 wt%) of well-dispersed GNPs can act as physical barriers that inhibit electrical treeing. During tree growth, the channels align and grow preferentially along the polymer/graphene interface, creating a “bush tree” pattern that propagates slowly within the matrix (Figure 7b). On the other hand, poorly dispersed GNPs at higher concentrations can create local highly conductive regions with reduced particle distances within clusters and dielectric strengths. In turn, tree channels propagate through these regions rapidly, causing lower degradation resistance and faster dielectric breakdown (Figure 7c). While the EVA/GNP blends used in this study were prepared by probe sonication and solution blending, local areas of GNP aggregates are still readily found throughout the blend (Figure 5). Hence, regions within the blend that contain clustered GNP agglomerates likely contribute to the electric treeing and dielectric breakdown of the composite under electric field application. Since the electrical treeing phenomenon is localized and occurs at a random location within the bulk sample, it is difficult to utilize imaging techniques such as TEM to directly observe treeing.

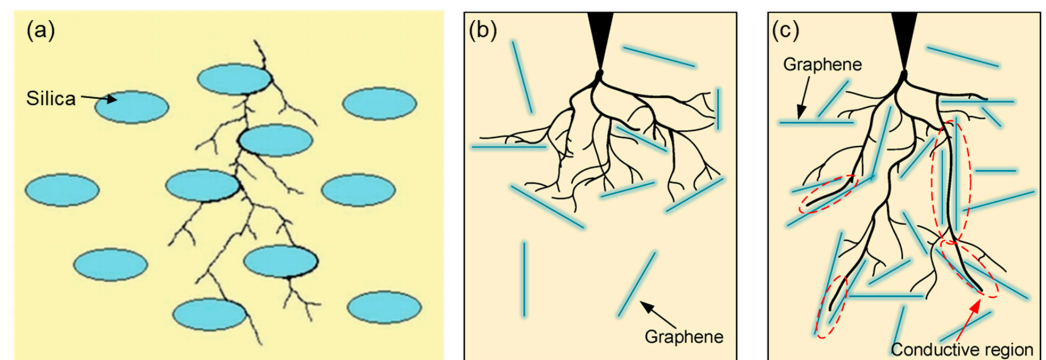


Figure 7. Schematic diagram of electric tree growth through (a) polymer/insulating silica particle composite with good particle dispersion, and (b,c) a polymer/graphene composite in which graphene within a local area is (b) at low concentrations and evenly dispersed or (c) at higher concentrations and poorly dispersed. In (a), tree growth proceeds in the area without particles but is hindered near the polymer/particle interface. Treeing process strongly depends on particle dispersion if conductive particles such as graphene are used. (b) Graphene is locally well-dispersed and tree formation is inhibited by electric field distortion along the polymer/graphene interface. (c) Local graphene agglomerates create locally conductive regions (highlighted in red) with lower dielectric strength that accelerate electrical treeing. Figure (a) is adapted with permission from Ref. [3]. Copyright © 2009, IEEE. Figures (b,c) are adapted with permission from Ref. [27]. Copyright © 2019 by the authors.

4.3. Parameters That Could Influence Dielectric Breakdown under Electric Field

We lastly measured the evolution of electrical conductivity as a function of time when EVA/GNP composites were subject to an applied electric field up to the point of dielectric breakdown. We systematically varied electric field strength (Figure 4a), matrix viscosity (Figure 4b), or GNP concentration (Figure 4c) in order to understand factors that could influence the rate of dielectric breakdown within these composites.

The growth in electrical conductivity of EVA/GNP composites under the external electric field undergoes three stages. Initially, the sample conductivity is low because the GNP concentrations of all samples were well below the percolation threshold in EVA (~0.6 wt%). Thus, the current signal was below the resolution of the high voltage sequencer (~10 μ A, corresponding to $\sim 2 \times 10^{-8}$ S/cm). Next, as the electric field induced the rotation and translation of individual GNP sheets, there was a sharp insulator to conductor transition. Lastly, the current growth appeared to be self-limiting upon nearing the current limit of the sequencer (~1 mA, corresponding to $\sim 3 \times 10^{-6}$ S/cm). At that stage, electric treeing had presumably already created a conductive pathway across the specimen thickness and dielectric breakdown is occurring. Here, we implement a simple logistic model to describe the progressive dielectric; similar models were used to describe the breakdown of metal-oxide semiconductors [28]. The simple three-parameter logistic growth model of the composite's electrical conductivity $\sigma(t)$ is constructed as follows:

$$\sigma(t) = \frac{\sigma_0}{1 + e^{-(t-t_0)/\tau}} \quad (5)$$

where σ_0 is maximal conductivity prior to dielectric breakdown, t_0 is the critical time when the rate of conductivity increase is the highest, and τ is the characteristic duration for which the conductivity grew from $0.1\sigma_0$ to $0.9\sigma_0$ [28]. Fitting results are summarized in Table 1. Overall, the logistic model provides an adequate fit to the electrical conductivity growth of EVA/GNP composites, especially after the onset of the sharp increase in the electrical conductivity. During the early stage of electric field application, the measured electrical conductivity is subject to higher variability and uncertainty. Possible reasons include sample-to-sample variability such as sample surface roughness and defects, and imperfect contact with the Cu electrode. These factors could all affect the probability of tree inception. Nonetheless, the simple logistic model offers important insights into the effects of field strength and filler concentration on the dielectric breakdown of polymer/graphene composites.

Table 1. Fitting results of logistic growth model, Equation (5), describing conductivity growth in EVA/GNP composites at 160 °C (numbers in parentheses represent the standard deviation across different samples).

w_{GNP} (wt%)	E_0 (V _{rms} /mm)	Number of Samples	σ_0 (S/cm)	τ (S/cm)	t_0 (s)
0.25	400	3	$1.7_{(0.4)} \times 10^{-6}$	11.7 _(2.3)	48.1 _(12.7)
0.25	250	2	$1.1_{(0.3)} \times 10^{-5}$	31.5 _(0.4)	136 _(24.6)
0.10	400	5	$9.2_{(5.6)} \times 10^{-6}$	149 ₍₁₀₀₎	640 ₍₁₀₇₎
0.05	400	1	2.0×10^{-7}	1230	6870

We could establish several general observations from our results. When GNP concentration was near or above the percolation threshold (~0.5 wt%), EVA/GNP underwent instantaneous runaway increase in electrical conductivity when the field was turned on. As these samples were instantaneously broken down, conductivity measurements could not be obtained. When the particle loading is above the percolation threshold, local conductive pathways already exist in the bulk sample. As such, electric treeing proceeds through the conductive regions with lower dielectric strengths and leads to early onset of dielectric breakdown. Additionally, t_0/τ , which is the ratio between the time of fastest conductivity growth and the characteristic duration falls within a narrow range of 4.1–4.3. In the subse-

quent discussion, we use parameter τ , the characteristic duration of conductivity growth, to describe the effect of the electric field leading towards the eventual dielectric breakdown of the composite. For the lowest concentration of the 0.05 wt% GNP sample, a slightly lower $\sigma_0 = 2.0 \times 10^{-7}$ S/cm and higher $t_0/\tau \sim 5.6$ were found.

First, we study the effect of the electric field strength on the dielectric breakdown when GNP concentration was fixed at 0.25 wt%. According to Table 1, τ measured at $E_0 = 250$ V_{rms}/mm was ~ 2.7 times the value compared to when $E_0 = 400$ V_{rms}/mm. Even though direct evidence of GNP alignment was not observed in TEM, the characteristic duration of conductivity growth similarly scaled with both the rotation and translation time of individual GNP sheets under the electric field on the basis of Equations (2) and (3), t_r and $t_c \sim \eta/E_0^2$. Given the experiments were performed at the same temperature of 160 °C, the viscosity of the EVA is identical across all samples. Therefore, the individual particle rotation and translation time between the two datasets would be inversely proportional to the square of the electric field strength, i.e., $[(250 \text{ V}_{\text{rms}}/\text{mm})/(400 \text{ V}_{\text{rms}}/\text{mm})]^{-2} = 2.56 \approx 2.7$.

Next, the effect of matrix viscosity on the dielectric breakdown is studied by varying the temperature of the composite melt during electric field application. In Table 2, we report the zero-shear melt viscosity of the EVA matrix at temperatures between 120 and 160 °C based on small-amplitude oscillatory shear measurements. By fitting τ obtained from the three-parameter logistics model given by Equation (5), as a function of different melt viscosities, we find the approximate relationship of $\tau \sim \eta$ (see Figure A2). This also empirically agrees with the theory related to the rotation and translation of individual GNP under the electric field, i.e., t_r and $t_c \sim \eta/E_0^2$. Therefore, the result suggests that the rate of conductivity increase could be related to the rate of individual conductive particles' motion within the composite. The electric field induces motion to anisotropic conductive fillers to form a local conductive pathway, which in turn leads to a reduction in the dielectric strength to cause dielectric breakdown. Differences in the initiation time of electrical conductivity increase between different samples under similar processing conditions may arise from the inherent sample-to-sample variations in GNP dispersion and sample contact with the test electrodes.

Table 2. Fitting results of the logistic growth model, Equation (5), describing conductivity growth in EVA/GNP composites with varying composite melt viscosities (numbers in parentheses represent the standard deviation across different samples).

w_{GNP} (wt%)	T (°C)	η (Pa·s)	σ_0 (>S/cm)	τ (s)	t_0 (s)
0.25	160	530	$1.7_{(0.4)} \times 10^{-6}$	11.7 _(2.3)	48.1 _(12.7)
0.25	140	1140	8.6×10^{-6}	30.7	910
0.25	130	1650	9.7×10^{-6}	26.6	1060
0.25	120	2430	7.0×10^{-6}	74.2	1290

Lastly, we observed that τ dramatically decreased with increasing GNP concentration at fixed electric field strength of 400 V_{rms}/mm. The rate of conductivity increase was much slower for blends with lower GNP concentration of 0.10 and 0.05 wt% (Figure 4c). Blends with higher GNP concentration exhibited shorter average interparticle distance. The lower concentration of the conductive filler species within the blend reduces the probability of the growth of electric treeing structure through conductive regions. Accordingly, blends with 0.10 or 0.05 wt% GNP were able to withstand eventual dielectric breakdown for longer duration (~ 25 – 60 min) as opposed to ~ 2 – 3 min in EVA/GNP_0.25 wt% blends. For GNP concentrations above 0.1 wt%, σ_0 reached at least 10^{-7} S/cm despite GNP concentration being well below the percolation threshold. The dramatic enhancement in the maximal electrical conductivity may indicate the formation of conductive pathway from electrical treeing during electric field application. While the origin of dielectric breakdown during electric field application is presumably dominated by the local electric treeing formation, blends with higher GNP concentration are more probable to exhibit locally conductive

regions that can favor treeing propagation. Results from Table 1 show that doubling GNP concentration leads to an approximate order-of-magnitude reduction in τ .

5. Conclusions

In this work, we studied the effect of an alternating electric field on the electrical conductivity of polymer/graphene composites. Applying an electric field up to 400 V_{rms}/mm to EVA/GNP composites in the melt greatly increased their electrical conductivity to $\sim 10^{-6}$ S/cm, despite filler concentrations below the percolation threshold. While a theory predicts that an alternating electric field induces rotation and translation motion to anisotropic filler particles loaded in an insulating polymer matrix, we did not observe global particle alignment in the field direction through TEM imaging. Instead, visual inspection revealed that samples underwent dielectric breakdown. We attribute the origin of the dielectric breakdown to the propagation of electrical trees. Local GNP agglomerates increase electrical conductivity and lower the dielectric strength in those regions. This accelerates the channel formation of electrical trees during electric field application, ultimately leading to dielectric breakdown. We established a simple logistic growth model to describe the increase in electrical conductivity due to electrical tree formation as a function of time. Qualitatively, the electrical conductivity of EVA/GNP blends sees slower growth when the applied electric field strength was lower, the composite viscosity was higher, scaling as predicted by alignment of graphene due to the electric field. It is possible that the local alignment of a few random GNP sheets promotes electrical treeing of its surrounding polymer dielectric, which ultimately leads the dielectric breakdown of the polymer composite. Additionally, the characteristic duration of conductivity growth decreased exponentially with increasing GNP concentration. The very low concentration of well-dispersed graphene could delay treeing by forming a tree bush around isolated particles. However, our blends with higher GNP concentration exhibited shorter interparticle distance and contained more locally conductive regions with GNP aggregates that favor electrical treeing propagation. Even though the mechanism of electric conductivity growth within EVA/GNP composites was complicated by the nonuniform dispersion of GNPs, our model could be adapted to other polymer/GNP systems to establish the scaling relationship between nanocomposite properties, and the degradation and breakdown dynamics under an applied electric field.

Author Contributions: Conceptualization, Y.K.; formal analysis, Y.K.; funding acquisition, X.C. and C.W.M.; investigation, Y.K.; methodology, Y.K.; resources, X.C. and C.W.M.; supervision, X.C. and C.W.M.; visualization, Y.K.; writing—original draft, Y.K.; writing—review and editing, Y.K., X.C. and C.W.M. All authors have read and agreed to the published version of the manuscript.

Funding: This research was funded by the United States National Science Foundation grant number CMMI-1661666. The authors acknowledge partial funding by the University of Minnesota Industrial Partnership for Research in Interfacial Materials and Engineering (IPRIME), and the University of Minnesota Rheology Short Course.

Institutional Review Board Statement: Not applicable.

Informed Consent Statement: Not applicable.

Data Availability Statement: Not applicable.

Acknowledgments: Parts of this work were carried out in the characterization facility of the University of Minnesota, a member of the NSF-funded Materials Research Facilities Network (www.mrfn.org, accessed on 6 May 2022) via the MRSEC program.

Conflicts of Interest: The authors declare no conflict of interest.

Appendix A

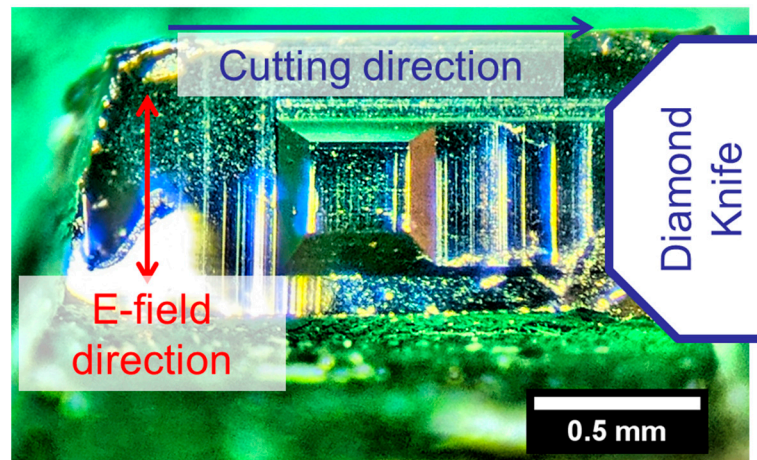


Figure A1. Determination of electric field direction based on sample orientation during cryomicrotomy. Cryomicrotomy was performed such that the diamond knife's cutting edge was parallel to the electric field direction. Knife marks were perpendicular to the field direction, and sample chattering patterns were parallel to the field direction.

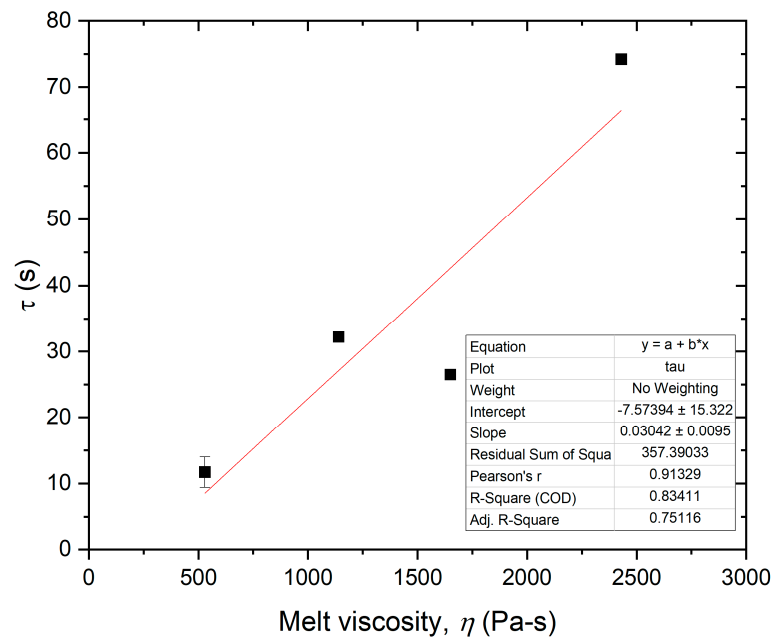


Figure A2. Fitting results between characteristic conductivity growth duration and melt viscosity of EVA/GNP_0.25 wt% composites under electric field strength of $400 V_{rms}/mm$.

References

1. Ding, S.; Yu, S.; Zhu, X.; Xie, S.; Sun, R.; Liao, W.-H.; Wong, C.-P. Enhanced Breakdown Strength of Polymer Composites by Low Filler Loading and Its Mechanisms. *Appl. Phys. Lett.* **2017**, *111*, 153902. [[CrossRef](#)]
2. Song, Y.; Shen, Y.; Liu, H.; Lin, Y.; Li, M.; Nan, C.-W. Improving the Dielectric Constants and Breakdown Strength of Polymer Composites: Effects of the Shape of the BaTiO₃ Nanoinclusions, Surface Modification and Polymer Matrix. *J. Mater. Chem.* **2012**, *22*, 16491. [[CrossRef](#)]
3. Danikas, M.G.; Tanaka, T. Nanocomposites—a Review of Electrical Treeing and Breakdown. *IEEE Electr. Insul. Mag.* **2009**, *25*, 19–25. [[CrossRef](#)]
4. Tanaka, T.; Iizuka, T. Generic PD Resistance Characteristics of Polymer Nanocomposites. In Proceedings of the 2010 Annual Report Conference on Electrical Insulation and Dielectric Phenomena, West Lafayette, IN, USA, 17–20 October 2010; pp. 1–4. [[CrossRef](#)]

5. Nurmi, S.; Hammi, T.; Demoulin, B. Protection Against Electrostatic and Electromagnetic Phenomena. In *Multifunctional Barriers for Flexible Structure*; Springer: Berlin/Heidelberg, Germany, 2007; pp. 63–83. [\[CrossRef\]](#)
6. Schwarz, M.K.; Bauhofer, W.; Schulte, K. Alternating Electric Field Induced Agglomeration of Carbon Black Filled Resins. *Polymer* **2002**, *43*, 3079–3082. [\[CrossRef\]](#)
7. Wang, H.; Zhang, H.; Chen, G. Preparation of Unsaturated Polyester/Graphite Nanosheet Conducting Composite under Electric Field. *Compos. Part A Appl. Sci. Manuf.* **2007**, *38*, 2116–2120. [\[CrossRef\]](#)
8. Wang, H.; Zhang, H.; Zhao, W.; Zhang, W.; Chen, G. Preparation of Polymer/Oriented Graphite Nanosheet Composite by Electric Field-Inducement. *Compos. Sci. Technol.* **2008**, *68*, 238–243. [\[CrossRef\]](#)
9. Chen, G.; Wang, H.; Zhao, W. Fabrication of Highly Ordered Polymer/Graphite Flake Composite with Eminent Anisotropic Electrical Property. *Polym. Adv. Technol.* **2008**, *19*, 1113–1117. [\[CrossRef\]](#)
10. Ma, C.; Zhang, W.; Zhu, Y.; Ji, L.; Zhang, R.; Koratkar, N.; Liang, J. Alignment and Dispersion of Functionalized Carbon Nanotubes in Polymer Composites Induced by an Electric Field. *Carbon* **2008**, *46*, 706–710. [\[CrossRef\]](#)
11. Wu, S.; Ladani, R.B.; Zhang, J.; Bafekrpour, E.; Ghorbani, K.; Mouritz, A.P.; Kinloch, A.J.; Wang, C.H. Aligning Multilayer Graphene Flakes with an External Electric Field to Improve Multifunctional Properties of Epoxy Nanocomposites. *Carbon* **2015**, *94*, 607–618. [\[CrossRef\]](#)
12. Monti, M.; Natali, M.; Torre, L.; Kenny, J.M. The Alignment of Single Walled Carbon Nanotubes in an Epoxy Resin by Applying a DC Electric Field. *Carbon* **2012**, *50*, 2453–2464. [\[CrossRef\]](#)
13. Lim, C.-S.; Rodriguez, A.J.; Guzman, M.E.; Schaefer, J.D.; Minaie, B. Processing and Properties of Polymer Composites Containing Aligned Functionalized Carbon Nanofibers. *Carbon* **2011**, *49*, 1873–1883. [\[CrossRef\]](#)
14. Bai, L.; Sharma, R.; Cheng, X.; Macosko, C.W. Kinetic Control of Graphene Localization in Co-Continuous Polymer Blends via Melt Compounding. *Langmuir* **2018**, *34*, 1073–1083. [\[CrossRef\]](#) [\[PubMed\]](#)
15. Mun, S.C.; Kim, M.J.; Cobos, M.; Gu, L.; Macosko, C.W. Strategies for Interfacial Localization of Graphene/Polyethylene-Based Cocontinuous Blends for Electrical Percolation. *AIChE J.* **2019**, *65*, e16579. [\[CrossRef\]](#)
16. Kou, Y.; Cheng, X.; Macosko, C.W. Polymer/Graphene Composites via Spinodal Decomposition of Miscible Polymer Blends. *Macromolecules* **2019**, *52*, 7625–7637. [\[CrossRef\]](#)
17. Kou, Y.; Cote, A.T.; Liu, J.; Cheng, X.; Macosko, C.W. Robust Networks of Interfacial Localized Graphene in Cocontinuous Polymer Blends. *J. Rheol.* **2021**, *65*, 1139–1153. [\[CrossRef\]](#)
18. Perrin, F. Mouvement Brownien d'un Ellipsoïde (II). Rotation Libre et Dépolarisation Des Fluorescences. Translation et Diffusion de Molécules Ellipsoïdales. *J. Phys. Radium* **1936**, *7*, 1–11. [\[CrossRef\]](#)
19. Yasin, S.; Hussain, M.; Zheng, Q.; Song, Y. Large amplitude oscillatory rheology of silica and cellulose nanocrystals filled natural rubber compounds. *J. Colloid Interface Sci.* **2021**, *588*, 602–610. [\[CrossRef\]](#)
20. Hussain, M.; Yasin, S.; Akram, M.A.; Xu, H.; Song, Y.; Zheng, Q. Influence of Ionic Liquids on Structure and Rheological Behaviors of Silica-Filled Butadiene Rubber. *Ind. Eng. Chem. Res.* **2019**, *58*, 18205–18212. [\[CrossRef\]](#)
21. Hussain, M.; Yasin, S.; Memon, H.; Li, Z.; Fan, X.; Akram, M.A.; Wang, W.; Song, Y.; Zheng, Q. Rheological and Mechanical Properties of Silica/Nitrile Butadiene Rubber Vulcanizates with Eco-Friendly Ionic Liquid. *Polymers* **2020**, *12*, 2763. [\[CrossRef\]](#)
22. Siddabattuni, S.; Schuman, T.P.; Dogan, F. Dielectric Properties of Polymer–Particle Nanocomposites Influenced by Electronic Nature of Filler Surfaces. *ACS Appl. Mater. Interfaces* **2013**, *5*, 1917–1927. [\[CrossRef\]](#)
23. Prado, G.; Jagoda, J.; Lahaye, J. Smoke Formation by Combustion of Polymeric Materials. *Fire Saf. J.* **1978**, *1*, 229–235. [\[CrossRef\]](#)
24. Vogelsang, R.; Farr, T.; Frohlich, K. The Effect of Barriers on Electrical Tree Propagation in Composite Insulation Materials. *IEEE Trans. Dielectr. Electr. Insul.* **2006**, *13*, 373–382. [\[CrossRef\]](#)
25. Dissado, L.A.; Fothergill, J.C. *Electrical Degradation and Breakdown in Polymers*; The Institution of Engineering and Technology (IET): Stevenage, UK, 1992. [\[CrossRef\]](#)
26. Niemeyer, L.; Pietronero, L.; Wiesmann, H.J. Fractal Dimension of Dielectric Breakdown. *Phys. Rev. Lett.* **1984**, *52*, 1033–1036. [\[CrossRef\]](#)
27. Han, T.; Du, B.; Su, J.; Gao, Y.; Xing, Y.; Fang, S.; Li, C.; Lei, Z. Inhibition Effect of Graphene Nanoplatelets on Electrical Degradation in Silicone Rubber. *Polymers* **2019**, *11*, 968. [\[CrossRef\]](#)
28. Miranda, E.; Bandiera, L.; Cester, A.; Paccagnella, A. Logistic Modeling of Progressive Breakdown in Ultrathin Gate Oxides. In Proceedings of the Electrical Performance of Electrical Packaging (IEEE Cat. No. 03TH8710), Estoril, Portugal, 16–18 September 2003; pp. 83–86. [\[CrossRef\]](#)